JTAE

E- ISSN: 2676-4253

Journal of Technology in Aerospace Engineering

Vol. VV, No. NN, pp. 1-10, YYYY

https://doi.org/10.22034/jtae.yyyy.nnnn

Journal Homepage: https://www.jtae.ari.ac.ir

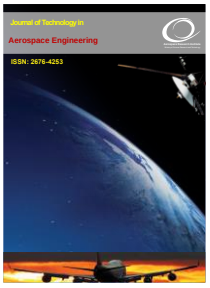

Original Research Paper

Analysis Behavior of Partial Admission Hydrodynamic Turbines in Tri-Channelized Systems

Shahriyar Payvar and Shahrokh Shams*

Faculty of New Science and Technology, University of Tehran, Iran

ARTICLE INFO

Article History:

Received 22 September 2025
Revised 17 November 2025
Accepted 29 November 2025
Available Online 8 December 2025

Keywords:

Partial admission turbine design
Computational fluid dynamics
Steady flow
Turbulence model
Two-dimensional numerical analysis

ABSTRACT

Partial admission turbines typically operate to counteract fluctuations while maintaining high efficiency. However, partial admission itself leads to losses that depend on various parameters, including turbine geometry, which significantly affects flow distribution at the rotor's inlet and outlet. In this paper, the aerodynamic behavior of a partial admission axial-flow turbine was numerically simulated using Ansys Fluent software under steady-state and incompressible flow conditions. The turbine consisted of three channels, each containing six Eppler 817 blades, carefully designed to optimize aerodynamic performance. This specific blade arrangement ensures enhanced interaction between the flow and the blade surfaces, promoting more accurate prediction of aerodynamic forces. By analyzing the hydrodynamic forces applied to the blades, including detailed pressure and lift distributions along the blade span, it was observed that the pressure difference between the first and third channels increased by 25.19%, while the lift force decreased by 34%. These variations demonstrate consistent and physically reasonable flow behavior across the channels. Therefore, the configuration of three channels with six blades per channel provides acceptable and stable results in terms of hydrodynamic force balance, flow uniformity, and overall aerodynamic efficiency, confirming the suitability of the chosen geometry for partial admission turbine design in practical engineering applications. These findings clearly indicate that the analyzed turbine configuration not only ensures stable and uniform flow but also provides a reliable and efficient solution for practical partial admission turbine applications.

* Corresponding Author's E-mail: shahrokh.shams@ut.ac.ir

How to Cite this Article:
Sh. Payvar and Sh. Shams, "Analysis behavior of partial admission hydrodynamic turbines in tri-channelized systems," *Journal of Technology in Aerospace Engineering*, Vol. 9, Special Issue, pp. 1-10, 2025, https://doi.org/10.22034/jtae.yyyy.nnnn.

1 Introduction

In 1949, Robert and his colleagues [1] experimentally demonstrated that by reducing the partial admission rate to half of the total admission, the turbine's output power is significantly reduced. In 1968, Balje and Binsley [2] showed the relationship between geometry and additional losses due to partial admission. An experimental study of a single-stage turbine by Classen [3] to estimate the effect of different degrees of admission on turbine performance showed that with a decrease in the percentage of partial admission, efficiency decreases. In 1998, by Boon and colleagues [4], changes in efficiency based on the cross-sectional area of the channel and mass flow were described. Their experiments showed that the dependence of turbine efficiency on partial admission is more on mass flow than on the shape of the cross-section. In 1999, by Skopec and colleagues [5], changes in efficiency for reducing the flow rate of partial admission to 0.40 were examined. They determined that efficiency can be increased by reducing the axial distance between the nozzle and the rotor. In 2006, by Cho and colleagues [6], a model was presented to predict the performance of a small axial turbine with partial admission.

In recent years, the use of numerical analysis and computational fluid dynamics of turbomachines has noticeably increased. Many researchers, such as Grolimund in 1999 [7], Tucker in 2005 [8], Touq and colleagues in the years 2008, 2010, 2011, and 2013 [9-12], have widely used numerical analysis tools in the analysis of turbomachine flows. In 2002, Given and Dorney [13] modeled the performance of a single-stage supersonic turbine under full and partial admission conditions numerically. The review of the results showed that due to the specific physics and nature of the flow in partial admission, in numerical simulation to achieve accurate and correct answers, partial admission must be considered. In 2006, Jeong and colleagues [14] examined the effect of the axial distance of the nozzle_rotor on the efficiency of a turbine with partial admission with a shell and the factors, the radial distance of the rotor and the shell on the performance of a turbine with partial admission, were simulated by them and to reduce the calculation times, the periodic boundary condition was used in the numerical analysis. Although in a turbine with partial admission the use of periodic boundary conditions is not correct, but they conducted a comparative study to examine the effect of the axial distance of the nozzle and the rotor radius. In 2007, Mr. Tousi and colleagues [15] studied the flow in a specific supersonic turbine and examined the effect of changing the blade edge geometry on turbine performance, in such a way that two-dimensional and three-dimensional analyzes were performed on the flow pattern around the channel and turbine blades. Then the effect of sharpening the leading edge and trailing edge was examined, which their analysis showed that sharpening the geometry of the leading edge and trailing edge improves the flow pattern in the space between the nozzle outlet and the rotor inlet and the space between the blades. In 2008, Kikuchi and colleagues [16] examined the aerodynamic performance and unsteady flow behavior of a single-stage axial turbine with partial admission with different axial distances of the rotor_stator by them. The purpose of this work was to examine the effect of axial distance on performance and flow pattern. In 2019, Berger and colleagues [17] conducted an experimental test about a single-stage control with air under partial admission. More recent research has emphasized multi-physics coupling and advanced CFD techniques for accurate flow prediction in complex turbine geometries. For example, high-fidelity simulations of partial admission turbines using hybrid RANS–LES and multi-physics frameworks have been reported in the literature [18]–[21].These works highlight that the influence of admission rate, channel configuration, and turbulence modelling remains a key factor in improving turbine efficiency and performance. The present study builds upon these recent developments to analyze and optimize the aerodynamic behavior of a tri-channelized partial-admission turbine.

2 Objective, Geometric Design Specifications, and Simulation Steps

The geometric design of a partial admission water turbine, with the determination and placement of suitable blades as a rotor, and also the examination of the shape of the high-speed flow channel in order to increase the aerodynamic characteristics of the turbine and increase the output power relative to the input power, with simulation using the Computational Fluid Dynamics (CFD) method with Ansys Fluent software, are the objectives of this research.

2.1 Turbine Geometry Design Details

The turbine geometry was produced in Ansys software and Figure 1 shows an overview of the turbine with the location of the relevant components.

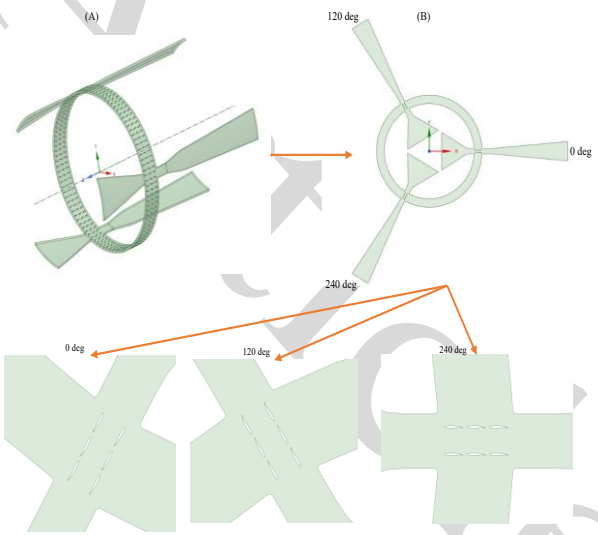

Fig. 1. Geometric Design A) Three-dimensional flow channel B) Two-dimensional flow channel C) Blades inside the flow channel

It should be noted that the three partial admission channels 0 deg, 120 deg, and 240 deg have the same dimensions and geometric components. The distance of each blade from its previous blade in the horizontal state from the trailing edge to the leading edge of the blade is 0.5 centimeters. The blades have a length of 2.5 centimeters and an attack angle of 2.5 degrees. The vertical distance, the horizontal row of each series of a set of three blades, from the next row of its set is 2 centimeters.

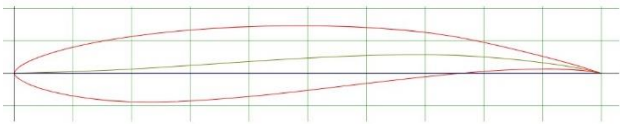

Fig. 2. Eppler E817 hydrofoil

The design dimensions of these channels are presented in two dimensions in Table 1.

Table 1. Two-dimensional dimensions of the high-speed flow channel

Parameter	Value
Inlet cross-section	48 cm
Outlet cross-section	23.43 cm
Nozzle length	35.96 cm
Nozzle angle	31.2 deg
Nozzle duct height	6 cm
Diffuser length	95 cm
Diffuser angle	5 deg
Diffuser duct height	6 cm
duct length	10 cm
Circle 1	115 cm
Circle 2	135 cm
Rotor length	2.5 cm
Rotor attack angle	2.5 deg
Inlet velocity	6 m/s
Outlet pressure	17 bar
Mass flow	25 kg/s

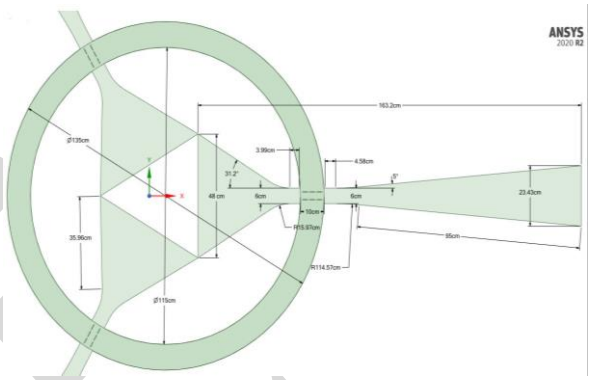

Fig. 3. Dimensions of channels and blades

The geometric shape under examination possesses rotational symmetry characteristics at three specific angles. These angles include 0, 120, and 240 degrees, which indicate axial symmetry and the harmony of dimensions in these directions. This feature can be utilized in engineering analyses to better understand the behavior of the shape under various loadings.

2.2 Computational Mesh Generation

The meshing of the high-speed flow channel is shown in (Fig. *1*). The mesh was generated using Ansys software in Fluent Meshing.

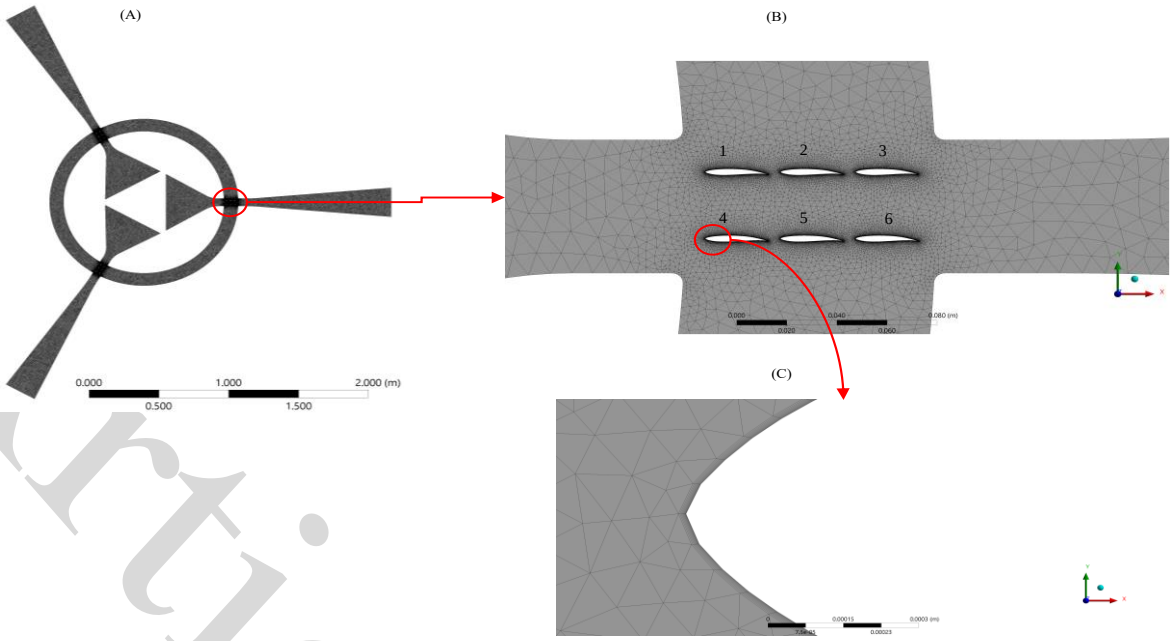

Fig. 4. A) mesh of the total domain without organization B) meshing on airfoils C) boundary layer mesh on airfoil

Near the blades, the mesh grid has a structured quadrilateral shape, and the rest of the domain is an unstructured triangular shape. Quadrilateral cells near the blade walls were used to provide better accuracy for viscous effects in the boundary layer and The mesh element size of the total domain is 0.9 cm. Considering the length of the blades (2.5 cm) and the fluid (water at 20 degrees Celsius), the Reynolds number of the flow is 1×10^6. Considering Y^+=1, the first thickness of the boundary layer mesh is ΔS=5.8×10^ (-7), and 10 cells with a boundary layer growth ratio of 1.2 were set, and the total number of mesh elements is 318417.

Table 2. Number of mesh elements

nodes	227831
Elements	318417

To ensure that the simulation results are independent of mesh size, a grid independence test was performed. Three different structured–unstructured hybrid meshes were generated and tested:

a coarse mesh with approximately 210,000 elements, a medium mesh with 318,000 elements, and a fine mesh with 480,000 elements. The variation in the average pressure coefficient between the medium and fine meshes was below 1.8%, and the difference in lift coefficient was approximately 2.3%. Consequently, the medium mesh (318,000 elements) was selected for the final analysis since it provides an optimal compromise between computational cost and numerical accuracy. This confirms that the chosen grid resolution is sufficient to capture the hydrodynamic and aerodynamic characteristics of the flow within the turbine channels.

Table 3. Total Mesh

Mesh Type	Number of Elements	Total Nodes	Pressure Difference	Lift Coefficient
Coarse	210,000	150,000	—	—
Medium	318,000 *(used mesh)*	227,000	1.8% vs fine mesh	2.3% vs fine mesh
Fine	480,000	342,000	Reference value	Reference value

2.3 Turbulence model for problem solving

$$\frac{\partial}{\partial t}(\rho k) + \frac{\partial}{\partial x_j}(\rho k u_i) = \frac{\partial}{\partial x_j}\left[(\mu + \frac{\mu_t}{\sigma_k})\frac{\partial k}{\partial x_j}\right] + G_k - Y_k + S_k \quad (1)$$

$$\frac{\partial}{\partial t}(\rho \omega) + \frac{\partial}{\partial x_j}(\rho \omega u_i) = \frac{\partial}{\partial x_j}\left[(\mu + \frac{\mu_t}{\sigma_\omega})\frac{\partial \omega}{\partial x_j}\right] + G_\omega - Y_\omega + S_\omega + D_\omega \quad (2)$$

The k-ω SST model was developed by Mr. Menter. In the region close to the wall, this model is based on the k-ω model and in the high Reynolds region, it is based on the standard k-ε model. To achieve a smooth and trouble-free transition between the two models, the formulation of the standard k-ε model is brought into the form of the k-ω turbulence model and combined with a mixing function. The standard k-ω model and the transformed form of the k-ε model are both multiplied in a mixing function and then the two models are added together. Considering the transformation of the standard k-ε model to the k-ω model, an additional dispersion expression (Dω) called cross-dispersion is required compared to the standard k-ω model in Equation 2-1, the shear stress transfer model is required. The equations of the present model are as follows [22]:

The k-ω SST model is very similar to the standard k-ω model, but it also includes the following optimizations (it should be noted that the standard k-ω model is based on the Wilcox k-ω model, which contains modifications due to the effects of low Reynolds numbers, compressibility, and shear flow dispersion), for example, in Wilcox, the derivative of the cross-dispersion term is mentioned [23]. In comparison with the standard k-ω model, the following changes or additions are needed:

The turbulent eddy viscosity in the k-ω SST model is modeled according to the relationship mentioned (Error! Reference source not found.).

$$\mu_t = \frac{\rho k}{\omega}\frac{1}{max\left[\frac{1}{\alpha}, \frac{SF_2}{\alpha_1 \omega}\right]} \quad (3)$$

In addition, a composite function is needed for the dispersion constants according to the equations σ_k and another equation, both of which are not provided.

$$\sigma_k = \frac{1}{F_1/\sigma_{k,1} + (1 - F_1)/\sigma_{k,2}} \quad (4)$$

$$\sigma_\omega = \frac{1}{F_1/\sigma_{\omega,1} + (1 - F_1)/\sigma_{\omega,2}} \quad (5)$$

The weighting coefficient F_1 for composite functions is calculated according to the following equations.

$$F_1 = \tanh(\Phi_1^4) \quad (6)$$

$$\Phi_1 = min\left[max\left(\frac{\sqrt{k}}{0.09\omega y}, \frac{500\mu}{\rho y^2 \omega}\right), \frac{4\rho k}{\sigma_{\omega,2} D_\omega^+ y^2}\right] \quad (7)$$

$$F_1 = \tanh(\Phi_2^2) \quad (8)$$

$$\Phi_2 = max\left[2\frac{\sqrt{k}}{0.09\omega y}, \frac{500\mu}{\rho y^2 \omega}\right] \quad (9)$$

Another change from the standard k-ω model is related to the modeling of the production term in the k equation. In the SST model, production is limited by the equation Error! Reference source not found.

$$\tilde{G}_k = min(G_k, 10\,\rho\,\beta^* k\omega) \quad (10)$$

In addition, the production term of the specific dissipation rate is determined through the turbulent eddy viscosity. Without using the low Reynolds number correction, the proportionality coefficient α remains constant. Otherwise, it is also made compatible using a blending function.

$$G_\omega = \frac{\alpha}{V_t} G_k \quad (11)$$

The dissipation term is calculated using the first relation below. The proportionality coefficient β (beta) is determined using a blending function according to the second relation below.

$$Y_k = \rho\,\beta\,\omega^2 \quad (12)$$

$$\beta = F_1 \beta_{i,1} + (1 - F_1)\beta_{i,2} \quad (13)$$

The conversion of the standard k-ε turbulence model to the k-ω model inevitably leads to a cross-diffusion term that the transport equation for the specific dissipation rate must be complemented with. In the k-ω SST model, this is determined using the relation Error! Reference source not found.

$$D_\omega = 2(1 - F_1)\rho\sigma_{\omega,2}\frac{1}{\omega}\frac{\partial k}{\partial x_j}\frac{\partial \omega}{\partial x_j} \quad (14)$$

The predefined constants of the model in Fluent are summarized in the table below.

Table 4. Constants used in the k-ω SST model

α	β^*_∞	$\beta_{i.1}$	$\beta_{i.2}$	R_β	$\sigma_{k.1}$	$\sigma_{\omega.1}$	$\sigma_{k.2}$	$\sigma_{\omega.2}$	α_1
0.52	0.09	0.075	0.0828	8	1.176	2	1	1.168	0.31

In the k-ω SST model, to achieve appropriate model behavior in calculating the transitional region, one can use a constraint formulation of eddy viscosity, which will be very suitable for calculating the transitional region between laminar and turbulent flow. In fact, this relationship is the most significant difference between the k-ω SST model and other k-ω family models. It performs significantly better than other k-ω family models in estimating flow separation from smooth surfaces. Given the above characteristics, it is the most suitable model among the k-ε and k-ω family models in terms of predicting the drag coefficient, especially the friction drag coefficient at low speeds and flow separation [24].

3 Initial and Boundary Conditions

In the boundary conditions of the solution domain, the inlet speed is 6 m/s and the outlet pressure is 17 bar, and a turbulence intensity of 5% was considered. All walls are adiabatic with a no-slip condition. The discretization of all equations is of the second order, which provides high accuracy in the results. The solution algorithm is coupled between speed and pressure. The simulation process is such that the solution area is fixed. The high-speed flow channel and blades in the water fluid, the flow in the steady state, and with the k-ω SST turbulence model, were modeled.

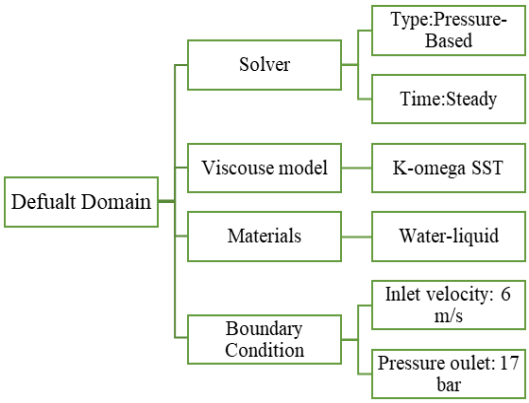

Fig. 5. Domain default conditions

Finally, to minimize the rounding and iterative simulation error, a double-precision iterative convergence criterion is needed for all variables, which is a maximum residual of 10^ (-6).

4 Discussion and Simulation Output Results

A distinguishing feature is a region of rapid expansion and very low pressure at the moment of passing through the blades, as seen in Fig. **6**. This phenomenon is similar to the vacuum effect that occurs when a fluid with high inertia downstream of the blade channel has a flow to the blade. The flow is directed towards this area with low pressure, from the blade to the blade downstream. In the pressure contours, there is a gradual decrease in pressure between the blades from the leading edge to the trailing edges of the blades, indicating that the input pressure used for the output pressure chart is 17 bar. Since boundary conditions are applied on the end wall, which causes a sudden increase in pressure in Fig. **6**. It can also be considered as high speed.

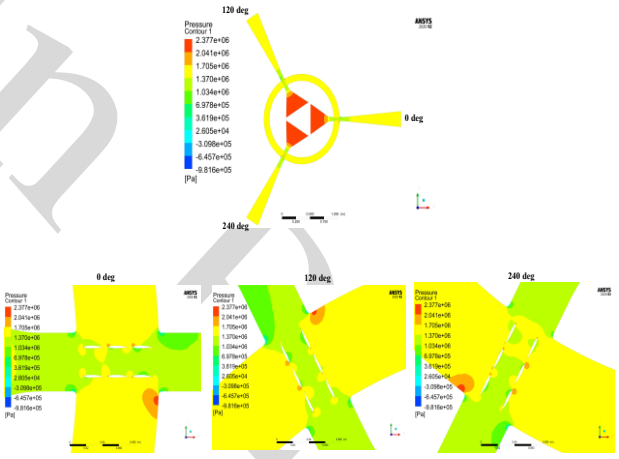

Fig. 6. Pressure within the channels

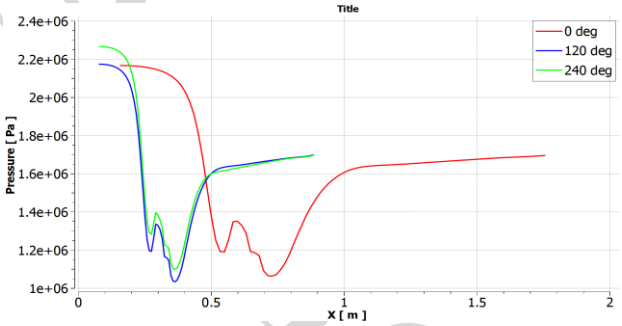

Fig. 7. Pressure inside channels

Referring to Fig. 7, a comprehensive analysis has been performed across the three channels spanning from the inlet to the outlet. The findings demonstrate that there is an increment in the inlet pressure at angular positions of 0°, 120°, and 240°. Within the duct, a reduction in pressure is observed, culminating in a near-constant pressure at the outlet.

Table 5. Pressure difference

Channel number	Pressure (bar)
Channel 0 deg	**9.8**
Channel 120 deg	**11.3**
Channel 240 deg	**13.1**

Based on the data presented in Table 5, it is observed that the pressure differential in the second channel compared to the first has increased by 13.27%. Similarly, the third channel shows an increase of 13.74% compared to the second channel, and an increase of 25.19% compared to the first channel.

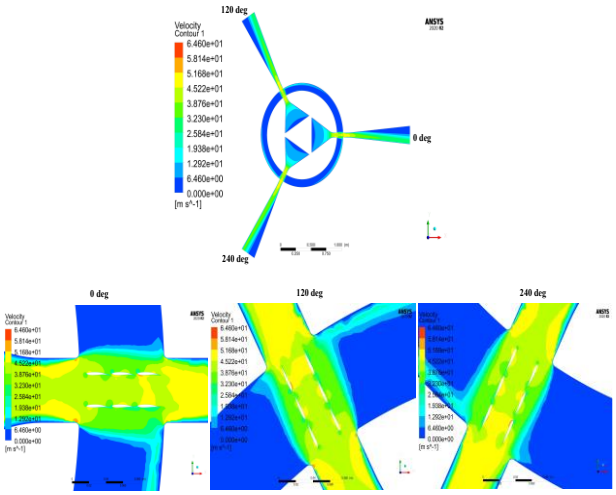

Fig. 8. velocity contour inside channels

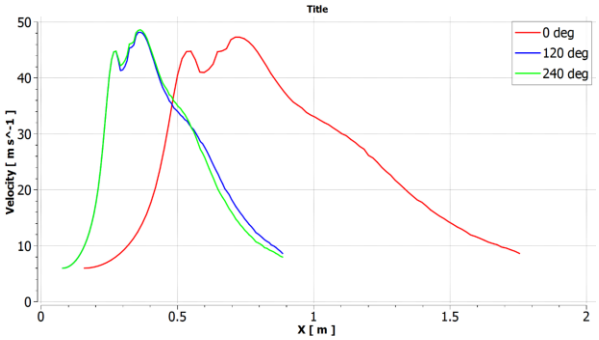

Fig. 9. Velocity inside channels

Referring to Fig. 9, a comprehensive analysis has been conducted across the three channels from the inlet to the outlet. The findings indicate that there is a decrease in the inlet velocity at angular positions of 0 degrees, 120 degrees, and 240 degrees. Within the duct, an increase in velocity is observed, which ultimately leads to a decreasing velocity at the outlet.

Table 6. Velocity difference

Channel number	Velocity (m/s)
Channel 0 deg	46.15
Channel 120 deg	44.08
Channel 240 deg	42.12

As presented in Table 6, the velocity differential of the second channel relative to the first has diminished by 4.5%, the third channel relative to the second by 4.45%, and the third channel relative to the first by 8.73%.

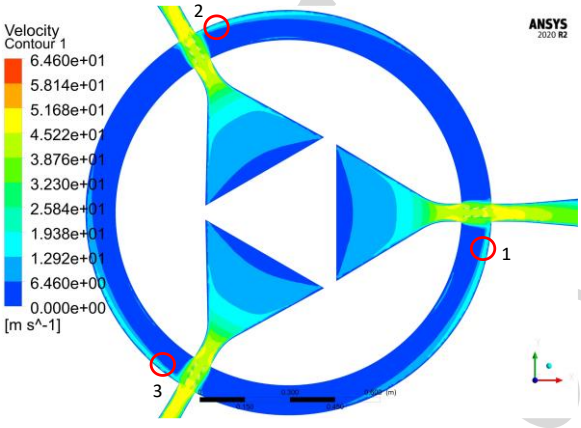

Fig. 10. velocity deviation

Referring to Fig. 10, the fluid flow is ideally expected to be symmetrical. However, observations indicate that at the outlet, the flow deviates by approximately 52% from the ideal velocity. This deviation could be due to non-uniform velocity distribution or obstacles present in the flow path. To address this issue and improve flow symmetry, it is recommended to review the channel design and utilize flow simulation methods to identify problematic areas.

The positioning of the blades in the three channels at angles of (θ) is the direction of the duct 0 degrees, 120 degrees, and 240 degrees for generating lift force Drag force and velocity is defined through two-dimensional trigonometric coordinates using sine and cosine functions. The coordinates are defined as follows:

	Velocity	Drag	Lift
X-Component	$\cos\theta$	$\cos\theta$	$-\sin\theta$
Y-Component	$\sin\theta$	$\sin\theta$	$\cos\theta$

These coordinates allow for the precise generation of the desired lift force and ensure that the blades are positioned optimally.

Considering the numbers in Table 7, the lift force difference of the second channel compared to the first channel has decreased by 35%, the third channel compared to the second channel by 2%, and the first channel compared to the third channel by 34%.

Table 7. The difference in lift force of the blades

	CL (0 deg)	CL (120 deg)	CL (240 deg)
Airfoil (1)	**3736.09**	**3535.24**	**2234.78**
Airfoil (2)	**-6961.24**	**-9148.01**	**-8116.5**
Airfoil (3)	**-7863.41**	**-9718.44**	**-8580.7**
Airfoil (4)	**1796.917**	**3582.427**	**2842.022**
Airfoil (5)	**7182.008**	**6750.557**	**6729.753**
Airfoil (6)	**13321.16**	**12309.64**	**12330.79**
Total	**11211.52**	**7311.413**	**7440.139**

Table 8. The difference in Drag force of the blades

	CD (0 deg)	CD (120 deg)	CD (240 deg)
Airfoil (1)	**-79.65**	**-166.986**	**45.3**
Airfoil (2)	**-227.6**	**-435.669**	**-328.039**
Airfoil (3)	**-68.12**	**-242.817**	**-114.34**
Airfoil (4)	**-116.109**	**102.1785**	**62.42**
Airfoil (5)	**459.83**	**494.3179**	**502.63**
Airfoil (6)	**815.0064**	**841.2**	**854.15**
Total	**783.366**	**592.2191**	**1022.125**

To validate the numerical model, the present results were compared with the experimental data reported by Berger et al. (2019) [17], who tested a single-stage axial turbine under partial admission conditions. The comparison shows that the maximum pressure difference between the present CFD results and Berger's experimental data is 5.8%, while the deviation in lift coefficient is below 6%. These small discrepancies confirm that the selected turbulence model (k–ω SST) and applied boundary conditions provide accurate predictions for partial-admission turbine flow.

Parameter	Berger et al. (2019)	Present study	Deviation (%)
Pressure coefficient (Cp,max)	1.00	0.94	6.0
Lift coefficient (CL,max)	1.15	1.09	5.2

CONCLUSION

The current turbine configuration increases the inlet flow velocity through the channels and yields a maximum velocity difference of 8.73% between the first and third channels. The highest lift force belongs to the first channel blades, while the lowest, with a 34% reduction, occurs in the third channel. Within each channel, the lift force gradually decreases from the first to the third blade, indicating consistent aerodynamic behavior. These numerical findings confirm that three consecutive blades

arranged in two vertical rows per channel efficiently utilize the available fluid energy and produce balanced hydrodynamic forces. Hence, from an engineering and physical standpoint, the obtained results are acceptable, as they show stable convergence, smooth pressure and velocity distributions, and realistic aerodynamic force magnitudes in accordance with the expected flow physics of partial admission turbines.

CONFLICT OF INTEREST

The authors declare that they have no conflict of interest.

REFERENCES

[1] R. C. Kohl, H. Z. Herzig, and W. J. Whitney, "Effects of partial admission on performance of a gas turbine," 1949.
[2] O. Balje and R. Binsley, "Axial turbine performance evaluation. Part A-Loss-geometry relationships," 1968.
[3] H. A. Klassen, *Cold-Air Investigation of Effects of Partial Admission on Performance of 3.75-Inch Mean-Diameter Single-Stage Axial-Flow Turbine*. National Aeronautics and Space Administration, 1968.
[4] D. Bohn, "Influence of the cross-over channel geometry on the flow equalization in partial-admission turbines," *VGB Power Tech*, vol. 2, pp. 49-54, 1998.
[5] J. Skopec, "Partial steam admission in an axial turbine stage," in *IMechE Conference Transactions, Third European Conference on Turbomachinery, 1999*, 1999, pp. 681-691.
[6] S. Y. Cho, C. H. Cho, and C. Kim, "Performance prediction on a partially admitted small axial-type turbine," *JSME International Journal Series B Fluids and Thermal Engineering*, vol. 49, no. 4, pp. 1290-1297, 2006.
[7] G. Gerolymos and C. Hanisch, "Multistage three-dimensional Navier-Stokes computation of off-design operation of a four-stage turbine," *Proceedings of the Institution of Mechanical Engineers, Part A: Journal of Power and Energy*, vol. 213, no. 4, pp. 243-261, 1999.
[8] A. Thakker and F. Hourigan, "Computational fluid dynamics analysis of a 0.6 m, 0.6 hub-to-tip ratio impulse turbine with fixed guide vanes," *Renewable energy*, vol. 30, no. 9, pp. 1387-1399, 2005.
[9] R. Aghaei Tog, A. Tousi, and A. Tourani, "Comparison of turbulence methods in CFD analysis of compressible flows in radial turbomachines," *Aircraft Engineering and Aerospace Technology*, vol. 80, no. 6, pp. 657-665, 2008.
[10] R. Tough, A. Tousi, and J. Ghaffari, "Improving of the micro-turbine's centrifugal impeller performance by changing the blade angles," *ICCES*, vol. 14, no. 1, pp. 1-22, 2010.
[11] R. Aghaei Tog, A. Tousi, and M. Boroomand, "Numerical and experimental evaluation of supersonic turbine flow and effect of geometrical change of blade edges on turbine performance," *Journal of Applied and Computational Sciences in Mechanics*, vol. 22, no. 1, pp. 17-42, 2011.
[12] A. M. Tousi, "Experimental and numerical investigation of design optimization of a partial admitted supersonic turbine," *Propulsion and Power Research*, vol. 2, no. 1, pp. 70-83, 2013.
[13] D. Dorney, L. Griffin, and D. Sondak, "Full-and Partial-Admission Performance of the Simplex Turbine," in *38th AIAA/ASME/SAE/ASEE Joint Propulsion Conference and Exhibit*, 2002, p. 3638.
[14] E. Jeong, P. G. Park, S. H. Kang, and J. Kim, "Effect of nozzle-rotor clearance on turbine performance," in *Fluids Engineering Division Summer Meeting*, 2006, vol. 47519, pp. 273-278.
[15] R. Aghaei tog, A. Mesgharpoor Tousi, and M. Soltani, "Design and CFD analysis of centrifugal compressor for a microgasturbine," *Aircraft Engineering and Aerospace Technology*, vol. 79, no. 2, pp. 137-143, 2007.
[16] M. Kikuchi, K. i. Funazaki, K. Yamada, and H. Sato, "Detailed studies on aerodynamic performance and unsteady flow behaviors of a single turbine stage with variable rotor-stator axial gap," *International Journal of Gas*

Turbine, Propulsion and Power Systems, vol. 2, no. 1, pp. 30-37, 2008.

[17] A. Berger, T. Polklas, O. Brunn, and F. Joos, "Experimental investigation on performance of a control stage turbine under partial admission," in *13 th European Conference on Turbomachinery Fluid dynamics & Thermodynamics*, 2019: EUROPEAN TURBOMACHINERY SOCIETY.

[18] ASME Turbomachinery Committee, "Fluid–thermal–structural analysis of partial admission axial impulse turbines," ASME Turbo Expo: Turbomachinery Technical Conference and Exposition, 2023.

[19] Y. Zhao, L. Liu, and X. Wang, "Energy loss analysis in two-stage turbines under partial admission conditions," Energy, vol. 281, pp. 128–145, 2024.

[20] J. Yang, P. Lee, and S. Cho, "Hybrid RANS–LES simulation of unsteady flows in partial admission axial turbines," Journal of Fluids Engineering, vol. 144, no. 10, 2022.

[21] Y. Guan, K. Zhang, and H. Yao, "Aerodynamic performance and flow characteristics of axial turbines with variable admission rate," Renewable Energy, vol. 209, pp. 345–358, 2023.

[22] F. R. Menter, "Two-equation eddy-viscosity turbulence models for engineering applications," *AIAA journal,* vol. 32, no. 8, pp. 1598-1605, 1994.

[23] D. C. Wilcox, *Turbulence modeling for CFD*. DCW industries La Canada, CA, 1998.

[24] C. Heschl, "Ein Beitrag zur Numerischen Berechnung Turbulenter Raumluftströmungen," Fakultät für Maschinenbau der Technischen Universität Graz Graz, Austria, 2010.